Am J Nucl Med Mol Imaging 2013;3(2):102-117
www.ajnmmi.us /ISSN:2160-8407/ajnmmi1301003

Original Article

Alzheimer's disease imaging with a novel Tau targeted near infrared ratiometric probe

Hye-Yeong Kim[1], Urmi Sengupta[2], Pin Shao[1], Marcos J Guerrero-Muñoz[2], Rakez Kayed[2], Mingfeng Bai[1,3]

[1]Molecular Imaging Laboratory, Department of Radiology, University of Pittsburgh, Pittsburgh, PA 15219, USA; [2]Departments of Neurology and Neuroscience & Cell Biology, George and Cynthia Mitchell Center for Neurodegenerative Diseases, University of Texas Medical Branch, Galveston, Texas 77555-1045, USA; [3]University of Pittsburgh Cancer Institute, Pittsburgh, PA 15213, USA

Received January 15, 2013; Accepted February 11, 2013; Epub March 8, 2013; Published March 18, 2013

Abstract: Neurofibrillary tangles (NFTs) have long been recognized as one of the pathological hallmarks in Alzheimer's disease (AD). Recent studies, however, showed that soluble aggregated Tau species, especially hyperphosphorylated Tau oligomers, which are formed at early stage of AD prior to the formation of NFT, disrupted neural system integration. Unfortunately, little is known about Tau aggregates, and few Tau targeted imaging probe has been reported. Successful development of new imaging methods that can visualize early stages of Tau aggregation specifically will obviously be important for AD imaging, as well as understanding Tau-associated neuropathology of AD. Here, we report the first NIR ratiometric probe, CyDPA2, that targets Tau aggregates. The specificity of CyPDA2 to aggregated Tau was evaluated with *in vitro* hyperphosphorylated Tau proteins (pTau), as well as *ex vivo* Tau samples from AD human brain samples and the tauopathy transgenic mouse model, P301L. The characteristic enhancements of absorption ratio and fluorescence intensity in CyDPA2 were observed in a pTau concentration-dependent manner. In addition, fluorescence microscopy and gel staining studies demonstrated CyDPA2-labeled Tau aggregates. These data indicate that CyDPA2 is a promising imaging probe for studying Tau pathology and diagnosing AD at an early stage.

Keywords: Near infrared (NIR), ratiometric, probe, Tau, Alzheimer's disease (AD), imaging

Introduction

Neurofibrillary tangles (NFTs) and β-amyloid (Aβ) plaques have been widely recognized as theneuropathological hallmarks of AD. Over last decades, primary diagnostic and therapeutic target in AD has been mainly focused on Ab aggregates [1-3]. The accumulated data have shown the lack of correlation of β-amyloid deposition and cognitive impairments in AD, which implies a complexity and other markers in AD neurophathology [4, 5]. Unlike β-amyloid plaque formations, human post-mortem studies show the quantitative relationship between NFT deposition and neurodegeneration in AD [6, 7]. Tau polymerization is known as a key mechanism in NFT development, which is consisted of hyperphosphorylated Tau (pTau) and plays important pathological roles in neurodegenerative tauopathies [8]. Tau aggregates are characterized by abnormal phosphorylation, which is a crucial cause of neuron cell death through Tau-mediated down regulations [9-12]. Increasing evidence of Tau in neurodegeneration supports Tau as a potential target for disease-modifying therapeutics in AD treatment [13-17]. Therefore, development of highly phosphorylated Tau protein-specific imaging probe is important in elucidating the pTau–associated neuropathology and for further imaging and therapeutic applications in AD.

Although few probes targeted to Tau aggregates have been reported, there have been several reports on NFT-targeted probes. Hamachi *et al.* developed BODIPY-based fluorescent probes for NFT detection [18], and thiohydantoin (TH) derivatives have been shown a high binding specificity to NFTs *in vivo* [19]. Recently, an ^{18}F-labeled PET ligand has been developed as a novel radiotracer for noninvasive Tau imaging which shows promising potentials for clini-

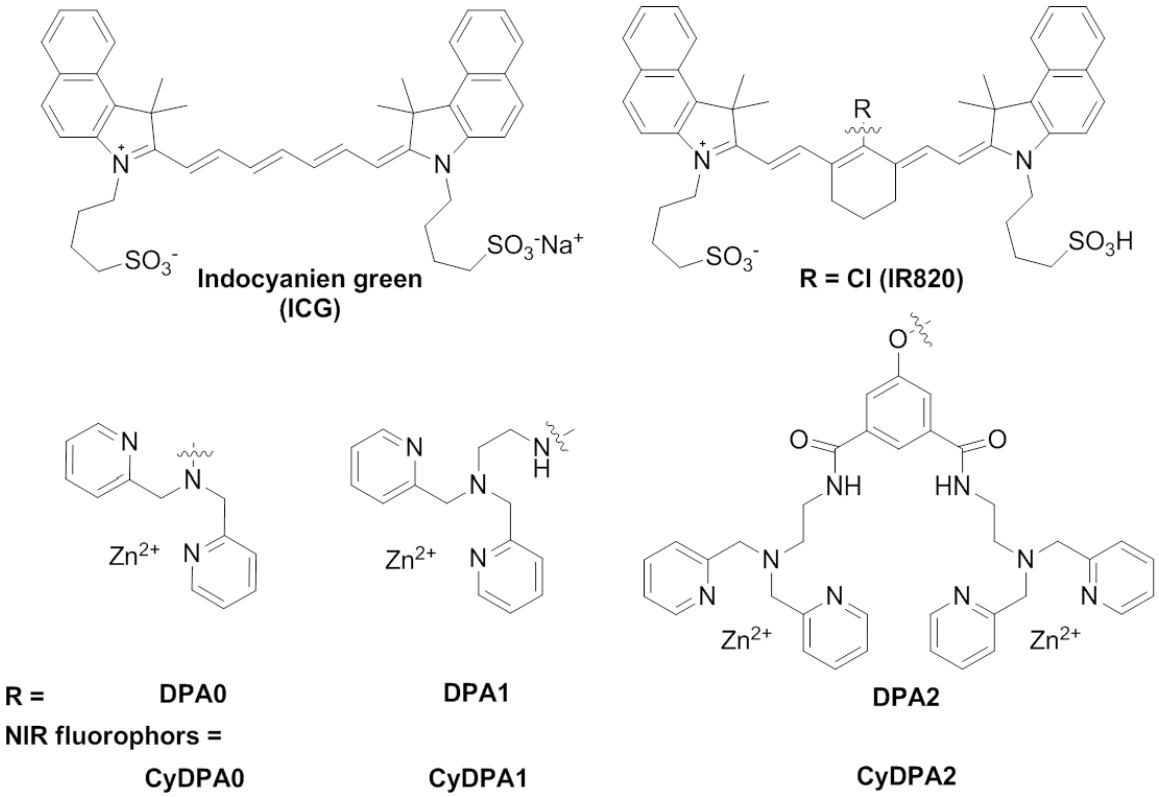

Figure 1. Chemical structures of Tau aggregates targeted NIR fluorophores (CyDPA).

cal phase trials [20]. In this study, we set out to develop near infrared (NIR) probes that bind to phosphorylated sites on Tau aggregates in early stages of NFTs formation. The NIR fluorophores are favorable for *in vivo* imaging due to the relatively low tissue absorption and negligible autofluorescence in the NIR window (650 - 900 nm) [21]. Typically, bound and unbound NIR probes have the same characteristic signal, and therefore, specific labeling of the target relies on both specific binding of the probes to the target sites and clearance of unbound probes from the living system. Ratiometric imaging, on the other hand, can discriminate bound and unbound NIR probes through measurement of absorption or emission ratio at two different wavelengths. Therefore, ratiometric imaging provides a significant advantage over conventional measurement at a single wavelength by allowing precise analysis even in complicated biological systems [22]. As such, we incorporated ratiometric signature in our probe design.

In this study, we report three NIR Tau aggregates targeted probes, CyDPA0, CyDPA1, and CyDPA2 (**Figure 1**). All three probes were designed based on the only FDA approved NIR dye, indocyanine green (ICG). Our protein binding, fluorescence microscopy and gel staining data demonstrated that CyDPA2 is a promising probe for Tau imaging. Moreover, the significant ratiometric signal change between bound and unbound CyDPA2 provides opportunities in imaging Tau pathology with high contrast, specificity and accuracy. To our knowledge, CyDPA2 is the first reported NIR ratiometric probe that targets Tau aggregates, with great potentials in AD research.

Materials and methods

General methods

All chemical reagents were purchased from commercial sources and used without further purifications, otherwise stated. DMF and DIPEA were distilled in the presence of CaH_2. Silica gel (240 - 400 mesh, Sorbtech) was used for column chromatography. NMR spectra were obtained from Bruker 400 MHz, and deutrated solvents were purchased from Cambridge

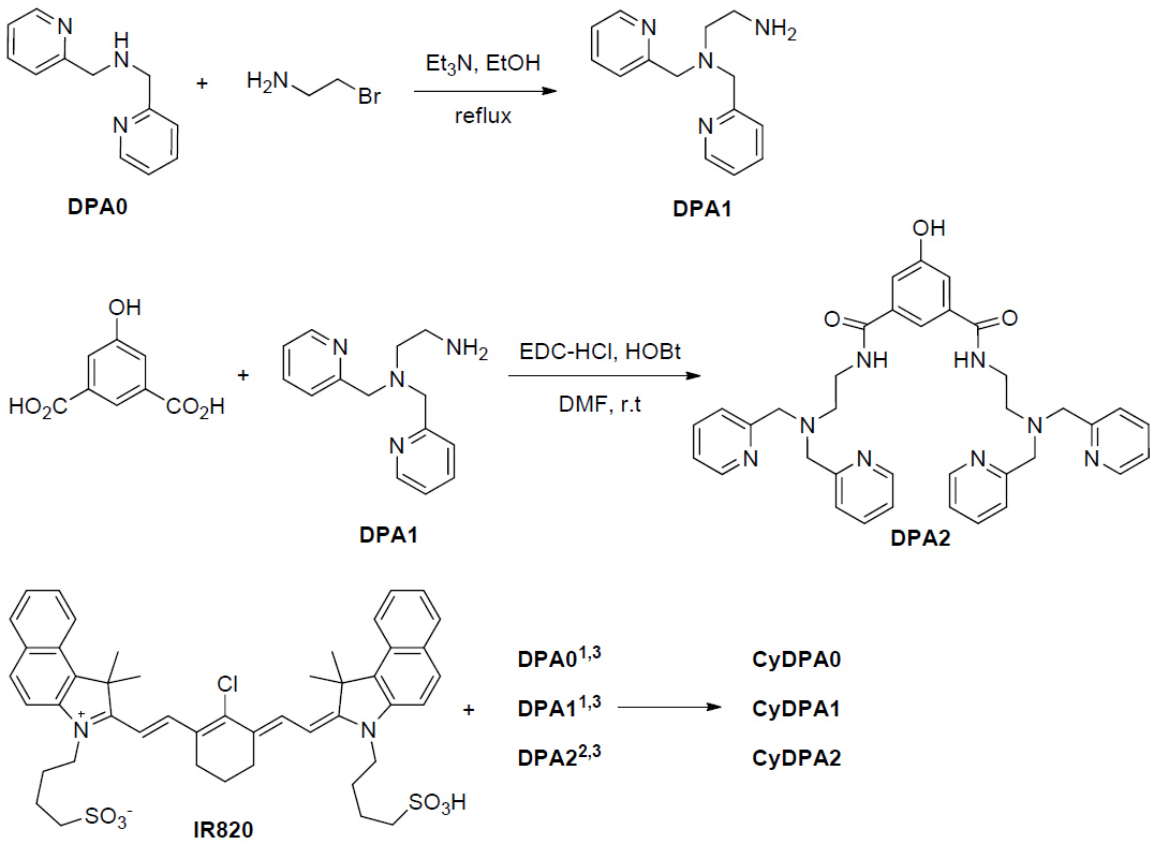

Figure 2. Synthesis of DPA derivatives and CyDPA conjugates. 1. DIPEA, DMF, 70°C, 5 hr; 2. i) DPA2, NaH, DMF, ii) DMF, R.T. 4 hr; 3. $Zn(NO_3)_2$, MeOH, R.T.

Laboratory (Andover, MA). FluoSpheres ($\lambda_{exi}/\lambda_{emi}$ = 535/575 nm, Molecular probes, Eugene, OR) was obtained from Invitrogen. Mass spectrometry was performed using ESI/MS (Waters 2998 photodiode array detector) and MALDI-TOF (Applied Biosystems, Voyager) using DHB (2, 5-dihydroxybenzoic acid) as a matrix.

Spectroscopy

Absorbance of compounds was measured using a Cary 100 Bio UV/Vis spectrophotometer. Fluorescence spectra were collected with a Cary Eclipse fluorescence spectrophotometer. Optical properties of compounds were measured using quartz fluorometer cuvettes (Starna cells, Inc., Atascadero, CA) at room temperature. The fluorescence quantum yields of all compounds were determined using ICG (Sigma, Φ = 0.13 in DMSO) and cresyl violet perchlorate (Acros, Φ = 0.59 in EtOH) as standards. The spectroscopic experiments with Tau proteins were performed using SynergyTM H4 Hybrid Multi-Mode microplate reader (BioTeck, Winooski, VT), and absorbance and emission were read at the wavelength of following.; CyDPA2 (5 μM, λ_{abs} = 750/810 nm, $\lambda_{exi}/\lambda_{emi}$ = 740/830 nm), CyDPA1 (15 μM, λ_{abs} = 630/730 nm, $\lambda_{exi}/\lambda_{emi}$ = 670/790 nm), and CyDPA0 (5 μM, λ_{abs} = 747 nm, $\lambda_{exi}/\lambda_{emi}$ = 730/810 nm). All solutions of proteins and CyDPA were freshly prepared in 50 mM HEPES containing 10% DMSO (pH 7.4) before mixing in a cuvette or in a 96-well plate.

Expression and purification of human recombinant full length Tau protein

Recombinant full–length human Tau protein (Tau 441, 2N4R, M.W. 45.9 kDa) was expressed and purified as described [23]. In brief, BL21 (DE3) strain of Escherichia coli bacterial cells were transformed with pET-28 plasmid and the cells were cultured in LB medium at 37°C under vigorous shaking. Once the protein from the bacterial cell pellet was eluted using cationic exchange column and subsequently purified using a Superdex column, it was tested in SDS-

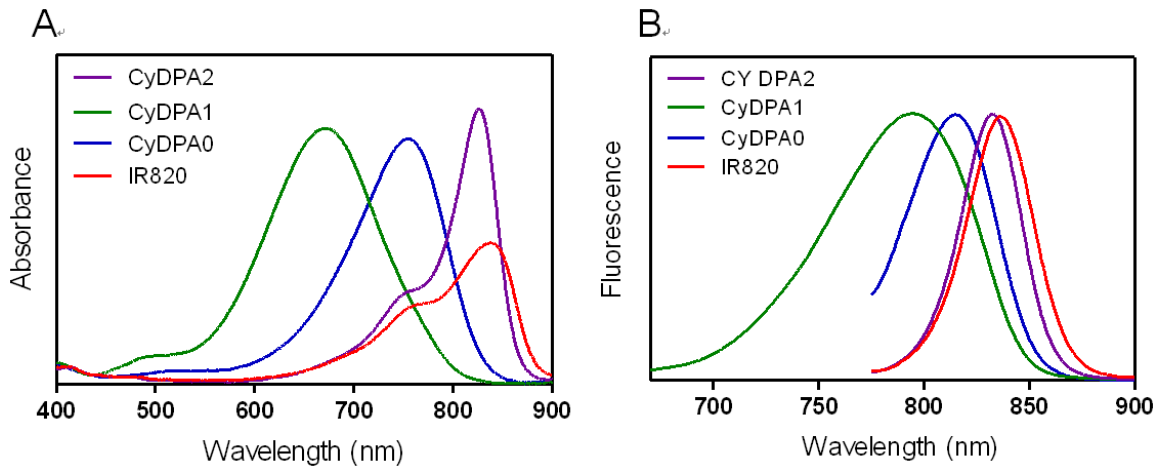

Figure 3. Normalized (A) absorption and (B) emission spectra of CyDPA0 (blue), CyDPA1 (green), CyDPA2 (purple), and IR820 (red) in DMSO.

PAGE gel. At this point the protein fraction was >95% pure and precipitated overnight with an equal volume of methanol at 4°C. The protein pellet was centrifuged at 10,000 X g, washed and stored in methanol and 2 mM DTT at -80°C until used.

Preparation of soluble Tau proteins (n,pTau)

The nTau protein pellet was dissolved in 50 mM HEPES and dialyzed (MWCO 10 kDa) against same buffer solution at 4 °C for 1 day. Phosphorylated Tau protein was prepared according to a known procedure [18]. Then, n,pTau concentrations were determined by BCA method (Thermo scientific Pierce, Rockford, IL) with BCA as a control, and the average percentage of phosphorylation was determined by Phosphoprotein Estimation Kit (Thermo scientific Pierce, Rockford, IL) with phosvitidine as a control.

Preparation of brain extracts

Frozen post-mortem brain tissue from patient with AD pathology was obtained from Institute for Brain Aging and Dementia (University of California-Irvine, Irvine, California, USA). JNPL3mice, Tg animal model expressing mutant human Tau protein P301L (Taconic Farms) that develop neurofibrillary tanlges (NFTs), amyotrophy and progressive motor disturbance were used here [24]. Brain tissues from AD patient (stage VI) and P301L mouse (10 months old) were prepared following the protocol as described [25]. Freshly prepared ice-cold 50 mM HEPES buffer (pH 7.4) containing protease inhibitor cocktail (Roche Applied Science, Indianapolis, IN, USA) was added to the brain tissues at a dilution of brain weight: buffer of 1:3 (w/v). Each tissue sample was homogenized using tissuelyzer and then centrifuged at 3,000 X g for 5 min at 4°C. The supernatant was aliquoted and stored at -80°C.

Gel electrophoresis and staining

AD brain extract (8 µg of total protein), P301L mouse brain extract (8 µg of total protein), pTau (0.7 µg), nTau (1.4 µg) and nTau protein (~ 6 µg) prepared from Tau pellet were run in the 4-12% bis-tris SDS-Page gel (Invitrogen). The gels were then incubated with 10 µM of CyDPA2 prepared in 10 mL of 50 mM HEPES, pH 7.4 with 10% DMSO for 10 min with gentle shaking at room temperature. Gels were washed twice with 50mM HEPES, pH 7.4 (each time washing for 10 min) on shaker and imaged with Kodak In-Vivo Multispectral Imaging System (FX PRO, Kodak). One gel was also stained with Pro-Q Diamond Phosphoprotein stain (Invitrogen) which specifically stains the phosphoproteins in polyacrylamide gels.

Fluorescence microscopy images

AD human brain homogenates, P301L mouse brain homogenates and nTau protein (1 µg in 20 µl for each) in buffer were applied onto Poly-L-lysine (PLL) coated coverslips (BD Biocoat) and dried in the sterilized hood for overnight. 100 µl of CyDPA2 (10 µM in 50 mM HEPES containing 10% DMSO, pH 7.4) containing 0.01% of FluoSpheres ($\lambda_{exi}/\lambda_{emi}$ = 535/575 nm) was gen-

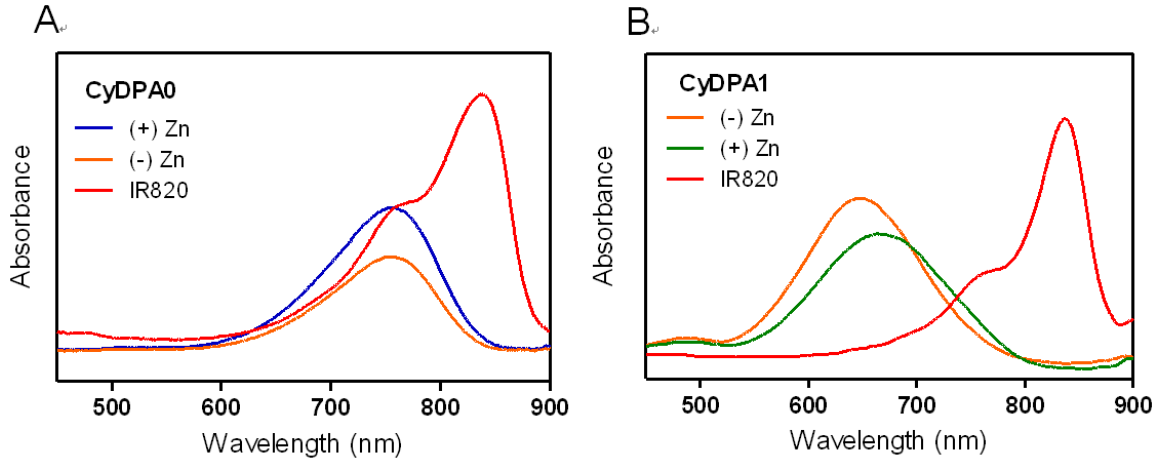

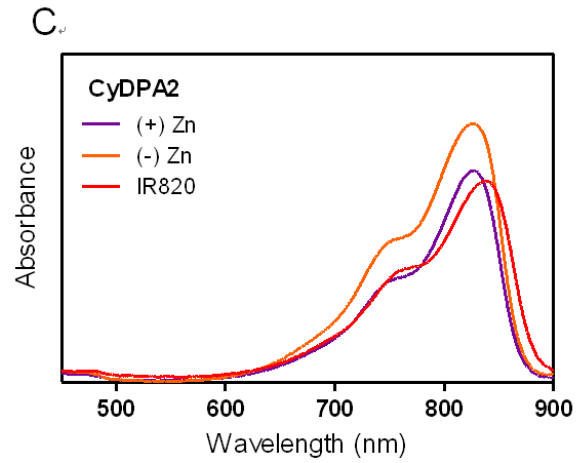

Figure 4. Absorption spectra of (A) CyDPA0, (B) CyDPA1, and (C) CyDPA2 with and without Zn^{2+} chelation in DMSO.

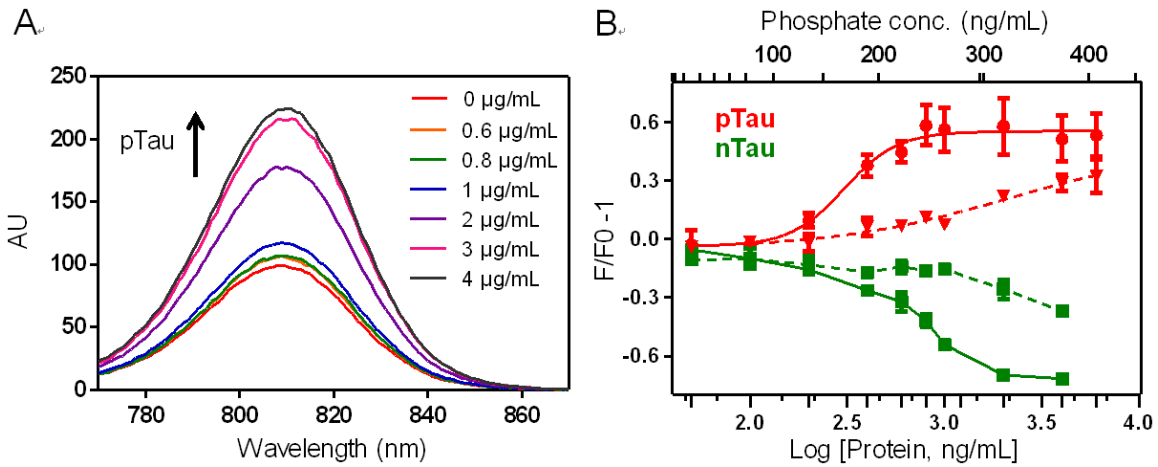

Figure 5. Fluorescence titrations of CyDPA2 (5 μM) and CyDPA1 (15 μM) in 50 mM HEPES containing 10% DMSO (pH 7.4). (A) Fluorescence spectral changes of CyDPA2 in pTau bindings (pTau: 0, 0.6, 0.8, 1, 2, 3, 4 μg/mL). (B) Fluorescence binding assay of CyDPA2 (solid line) and CyDPA1 (dashed line) with pTau (red) and nTau (green); 0, 0.05, 0.1, 0.2, 0.4, 0.6, 0.8, 1, 2, 4, 6, 12 μg/mL of n,pTau. Error bars represent s.d. of triplicates.

tly applied onto protein-coated cover slips and incubated for 10 min at room temperature under the dark. For phosphate blocking, 10 μM of CyDPA2 was prepared in 100 μM of ppi solution in 50 mM HEPES containing 10% DMSO, pH 7.4. After labeling, the coverslips were washed with 50 mM HEPES three times and mounted on glass slides. The microscopic fluo-

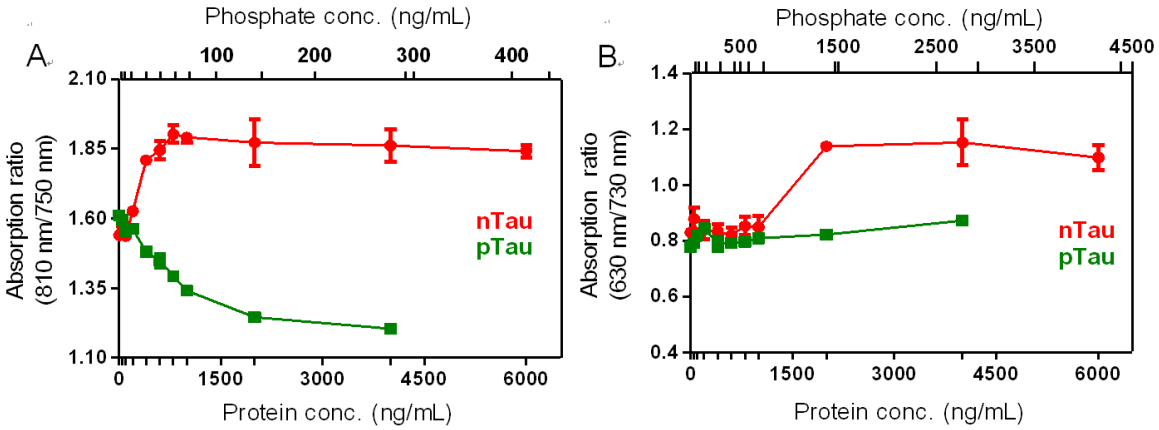

Figure 6. Ratiometric absorption changes of CyDPA2 and CyDPA1 with pTau and nTau titrations (0, 0.6, 0.8, 1, 2, 3, 4, 6 μg/mL) in 50 mM HEPES containing 10% DMSO (pH 7.4). Ratiometric absorption changes were obtained by measuring intensities at two wavelengths; (A) CyDPA2; at 810 nm and 750 nm; (B) CyDPA1; 630 nm and 730 nm. Error bars represent s.d. of triplicates.

rescence images were taken using a Zeiss Observer Z1 inverted microscope (Zeiss, Gottingen, Germany) and analyzed with Zen software.

General synthesis

Bis(2-pyridylmethyl)-amino)ethylamine (DPA1) [26] and IR820 [27] were synthesized by reported procedures. For Zn^{2+} chelation, equimolar amount of $Zn(NO_3)_2$ to DPA was mixed with CyDPA compounds in methanol (30 mM) and stirred for 30 min at room temperature. After evaporation of solvent, it was dried under vacuum. All dye stock solutions were prepared in DMSO and kept in -20 °C.

Bis-DPA-phenol (DPA2) [28]

5-Hydroxyisophthalic acid (100 mg, 0.459 mmol) was dissolved in CH_2Cl_2 (2 mL) followed by addition of DIPEA (0.1 mL) under argon. EDC/HCl and HOBt were added into the reaction mixture and stirred at room temperature for 10 min. Next, DPA1 (320 mg, 1.32 mmol) in CH_2Cl_2 (1 mL) was added dropwise into the reaction mixture, and the reaction mixture became a clear brown solution. After being stirred for 20 hr, the reaction mixture was partitioned between CH_2Cl_2 and saturated $NaHCO_3$ solution. The organic phase was then washed with water, dried with $MgSO_4$, concentrated with rotary evaporation and dried under vacuum to give brown oil in 28% yield. ^{1}H NMR (MeOD-d4, 400 MHz) δ 8.41 (m, 4H), 7.75 (t, 1H, J = 1.6 Hz, 1.2 Hz), 7.64 (td, 4H, J = 1.6 Hz, 7.6 Hz), 7.55 (d, 2H, J = 8 Hz) 7.20 (m, 4H), 3.82 (s, 8H), 3.55 (t, 4H, J = 6.0 Hz), 2.77 (t, 4H, J = 6.0 Hz, 5.6 Hz), ^{13}C NMR (DMSO-d6, 100 MHz) 169.25, 160.35, 159.36, 149.56, 138.64, 137.67, 125.10, 123.79, 118.24, 110.67, 60.90, 54.78, 38.87, M/S(ESI): calcd. For $C_{36}H_{38}N_8O_3$ $[M]^+$ m/z 630.31, found m/z 631.08 $[M+H]^+$, 316.07 $[M+2H]^{2+}$.

CyDPA0 [29]

IR820 (50 mg, 0.061 mmol) was dissolved in DMF (5 mL) followed by addition of DIPEA (0.5 mL) under argon. 2,2'-Dipicolylamine (146.8 mg, 0.606 mmol) in DMF (0.5 mL) was added dropwise into reaction mixture and heated at 70 °C for 5 hr. The dark brown mixture was precipitated out by addition of diethyl ether and the crude solid was purified by silica gel column chromatography (CH_2Cl_2/MeOH, 7:1, 3:1). Collected fraction was further purified by precipitation with diethyl ether to give blue powder form in 70% yield. ^{1}H NMR (DMSO-d6, 400 MHz) δ 8.81 (m, 2H), 8.18 (d, 2H, J = 8.4 Hz), 8.01 (d, 2H, J = 8.4 Hz), 7.91 (td, 2H, J = 2 Hz, 7.6 Hz), 7.78 (d, 2H, J = 14 Hz) 7.68 (d, 2H, J = 9.2 Hz), 7.64 (t, 2H, J = 7.2 Hz, 8 Hz), 7.51 (m, 2H), 7.45 (t, 2H, J = 7.2 Hz, 7.6 Hz), 7.35 (d, 2H, J = 8 Hz), 4.75 (s, 4H), 4.19 (bt, 4H), 2.61 (t, 4H, J = 6.2 Hz, 6.3 Hz), 2.53 (merged to solvent peaks, 4H), 1.84 (m, 4H), 1.73 (s, 12H), 13C NMR (DMSO-d6, 100 MHz) 170.58, 156.63, 150.13, 140.26, 137.45, 131.97, 130.75, 130.11, 129.9, 127.69, 127.53, 124.08, 124.05, 123.63, 123.17, 121.85, 111.40,

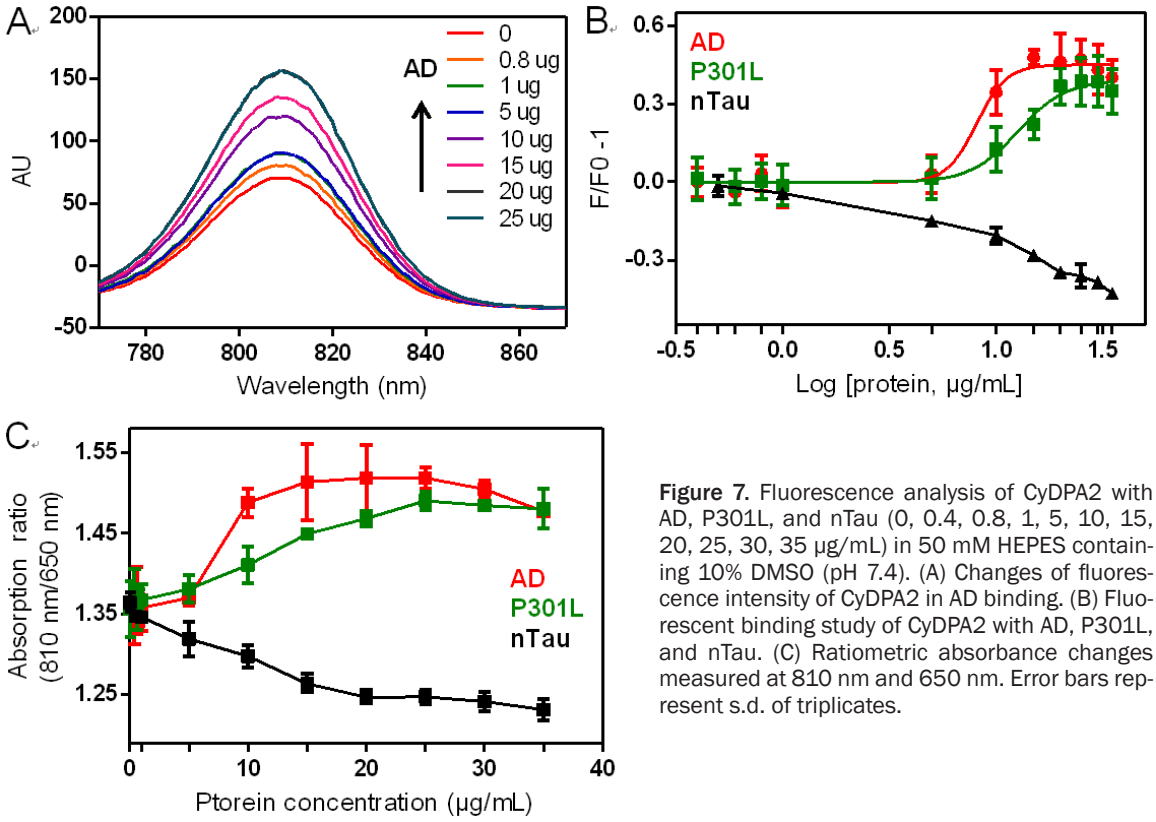

Figure 7. Fluorescence analysis of CyDPA2 with AD, P301L, and nTau (0, 0.4, 0.8, 1, 5, 10, 15, 20, 25, 30, 35 μg/mL) in 50 mM HEPES containing 10% DMSO (pH 7.4). (A) Changes of fluorescence intensity of CyDPA2 in AD binding. (B) Fluorescent binding study of CyDPA2 with AD, P301L, and nTau. (C) Ratiometric absorbance changes measured at 810 nm and 650 nm. Error bars represent s.d. of triplicates.

97.05, 59.82, 50.85, 49.58, 27.68, 25.98, 22.60; M/S MALDI-TOF: calcd. For $C_{58}H_{63}N_5O_6S_2$ $[M]^+$ m/z 989.42, found m/z 990.67 $[M+H]^+$.

CyDPA1 [30]

Same reaction method and scale as CyDPA0 was used for CyDPA1 synthesis. ^{1}H NMR (MeOD-d4, 400 MHz) δ 8.64 (m, 2H), 8.08 (d, 2H, J = 8.4 Hz), 7.97 (td, 2H, J = 1.4 Hz, 7.6 Hz), 7.89 (d, 4H, J = 8.8 Hz), 7.79 (d, 2H, J = 12.4 Hz), 7.62 (d, 2H, J = 7.6 Hz), 7.543 (m, 2H), 7.48 (m, 2H), 7.46 (d, 2H, J = 4.4 Hz), 7.36 (t, 2H, J = 7.6 Hz), 5.85 (d, 2H, J = 12.8 Hz), 4.23 (s, 4H), 4.10 (broad t, 4H), 3.91 (t, 2H, J = 6.4 Hz, 6 Hz), 3.17 (t, 2H, J = 6 Hz, 5.6 Hz), 2.583 (broad t, 4H), 1.981 (m, 4H), 1.838 (s, 12H); ^{13}C NMR (MeOD-d4, 100 MHz) 159.79, 150.19, 142.09, 138.72, 137.96, 132.39, 131.25, 131.03, 129.81, 128.16, 125.21, 124.61, 124.11, 122.86, 122.83, 111.35, 61.02, 55.23, 52.11, 50.47, 43.80, 28.45, 27.17, 23.69; MALDI-TOF: calcd. For $C_{60}H_{68}N_6O_6S_2$ $[M]^+$ m/z 1032.46, found m/z 1034.48 $[M+2H]^+$.

CyDPA2 [27]

Bis-DPA-phenol (91 mg, 0.14 mmol) in DMF (2 mL) was added into NaH (60% oil dispersion, 5.8 mg, 0.15 mmol) in DMF (2.8 mL) suspension under an Argon atmosphere. After being stirred at room temperature for 10 min, the bis-DPA-phenyl alkoxide solution was transferred to IR820 (100 mg, 0.11 mmol) in anhydrous DMF (5 mL) under an Argon atmosphere. The resulting mixture was stirred at room temperature for another 4 hours. After the solvent was removed by rotary evaporation, the crude product was purified by silica gel column chromatography with CH_2Cl_2/MeOH, and further purified by precipitation of its CH_2Cl_2 solution with diethyl ether. CyDPA2 was obtained as a green solid with a yield of 43%. ^{1}H NMR (MeOD-d4, 300 MHz) δ= 8.33 (d, 4H, J =4.8 Hz), 8.08-8.13 (m, 3H), 7.91-7.98 (m, 8H), 7.49-7.61 (m, 10H), 7.41-7.46 (m, 4H), 7.09 (t, 4H, J=9 Hz), 6.28 (d, 2H, J=14.4 Hz), 4.25 (br., 4H), 3.84 (s, 8H), 3.63 (t, 4H, J=5.7 Hz), 2.80-2.89 (m, 12H), 2.11 (br., 2H), 1.96 (br., 8H), 1.63 (s, 12H); ^{13}C NMR ($CDCl_3$, 100 MHz) δ= 203.05, 196.23, 192.08, 189.65, 188.37, 177.81, 170.10, 169.19, 166.99, 166.74, 163.22, 163.15, 161.57, 159.99, 159.27, 157.37, 156.78, 154.19, 153.27, 153.15, 151.93, 151.47, 151.30, 149.76, 146.21, 140.41, 129.33, 88.99, 82.84, 80.22, 79.91, 73.23, 67.28, 56.02, 55.64, 53.55, 51.71; MALDI-TOF: calcd. For

Table 1. Spectroscopic properties of CyDPA Zn(II) chelates in DMSO and aqueous solution

Compound	$\lambda_{Abs\ max}$ (nm)	ε ($M^{-1}cm^{-1}$)	$\lambda_{em\ max}$ (nm)[a]	Φ
In DMSO				
CyDPA2	826	113,553	833	0.049
CyDPA1	668	12,050	793	0.097[b]
CyDPA0	756	79,464	811	0.058
ICG	795	210,000	820	0.13
In 50 mM HEPES containing 10% DMSO				
CyDPA2	813	135,813	825	0.008
CyDPA1	698	8,675	796	0.031[b]
CyDPA0	748	82,533	810	0.037
ICG	782	64,640	807	

[a]λ_{ext} = 765 nm for CyDPA0 and CyDPA2; λ_{ext} = 578 nm for CyDPA1. [b]Quantum yield (Φ) was calculated using CVP (Cresyl violet perchlorate) as a reference.

$C_{82}H_{88}N_{10}O_9S_2$ $[M]^+$ m/z 1420.62, found m/z 1423.38 $[M+2H]^+$.

EC50 calculation

Dose-response curves were fitted to the fluorescence or ratiometric titration curves, and EC 50 values were calculated using GraphPad Prism software (version 5). EC50 value is defined as the effective concentration of Tau protein required to achieve 50% of the maximal fluorescence or ratiometric change.

Results

Synthesis of Tau aggregates targeted NIR fluorescence

Three individual NIR Tau aggregates targeted probes were designed and synthesized to optimize the pTau binding specificity and induce simultaneous ratiometric spectral changes (**Figure 1**). They share the same NIR fluorophore from a parent dye, IR820. Each NIR probe has one or two dipicolylamine DPA-Zn(II) complexes as the binding receptors to phosphate groups in pTau. We chose 2, 2'-dipicolylamine (DPA0) as the simplest mononvalent phosphate receptor for pTau detection. Ethylamine-elongated DPA (DPA1) was synthesized by a substitution reaction [26]. Binuclear DPA2 containing two DPA1 units was synthesized by conjugations of DPA1 to two carboxyl groups in 5-hydroxyisophthalic acid via a peptide coupling reaction. These phosphate-specific DPA-Zn(II) derivatives (DPA0, DPA1 and DPA2, **Figure 2**) were chemically introduced at close proximity to the center of the heptamethine (IR820) to generate ratiometic spectral changes. Previous studies have shown that binding of DPA-Zn(II) complexes to the target phosphorylated sites introduces coordination rearrangement of the Zn ions, resulting in a ratiometric spectroscopic change [22, 31, 32].

Here, three Tau aggregates targeted fluorophores, CyDPA0, CyDPA1 and CyDPA2, were synthesized from an ICG analog, IR820, by nucleophilic substitution (**Figure 2**) [33]. The vinyl chlorine on the heptamethine bridgehead of IR820 was replaced by secondary and primary amines on DPA0 and DPA1 respectively, in the presence of diisopropylethylamine (DIPEA). The neucleophilic phenoxide of DPA2 was generated *in situ* by treatment of NaH and transferred into the IR820 solution for a substitution reaction. During reaction, the formation of hypsochromicly shifted absorption peaks were observed from CyDPA0 (λ_{abs} = 756 nm), CyDPA1 (λ_{abs} = 668 nm) and CyDPA2 (λ_{abs} = 826 nm) substitutions (82 nm, 170 nm, and 12 nm respectively) compared to the IR820 (λ_{abs} = 838 nm in DMSO) (**Figure 3**). Such chromic shift allows the reaction progress to be monitored by an absorption change. Upon completion of reactions, these cyanine-DPA compounds were precipitated, purified by silica gel column chromatography, and characterized by NMR and mass spectrometry. After Zn^{2+} chelation, spectroscopic properties of Zn^{2+}-bound dye molecules were evaluated in both DMSO and aqueous media using UV/Vis and fluorescence spectrophotometers at ambient temperature (**Table 1** and **Figure 4**).

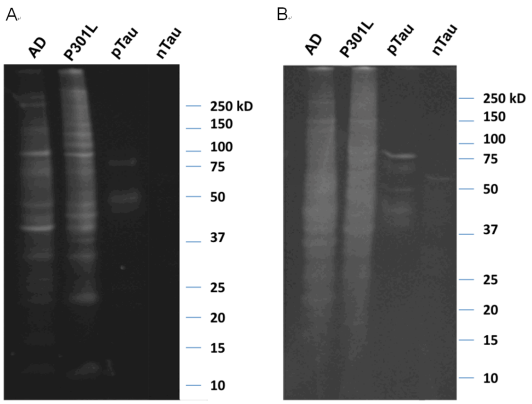

Figure 8. Gel images of AD, P301L, pTau, and nTau protein from (A) ProQ diamond staining and (B) CyDPA2 staining.

Absorption and emission changes upon pTau binding

We first evaluated the binding of CyDPA probes to phosphorylated full-length Tau protein. Hyperphorphorylated Tau (pTau) was synthetically prepared from non-phosphorylated Tau (nTau) according to a known procedure [18]. Briefly, the full-length Tau-441 protein (2N4R, 45.9 kD) was incubated with GSK-3β (glycogen synthase kinase-3β), and 7.4% of pTau was obtained from purified samples. Fluorescence titration studies of three CyDPA dyes were performed using nTau and pTau. The fluorescence intensity of CyDPAs increased upon pTau addition in a phosphate concentration-dependent manner, and a 2.3-fold increase of fluorescence was observed from CyDPA2 (**Figure 5A**). CyDPA2 (5 μM) showed the highest affinity to pTau with an EC50 value of 0.304 μg/mL corresponding to pTau (**Figure 5B**). EC50 value is defined as the effective concentration of Tau protein required to achieve 50% of the maximal fluorescence or ratiometric change. Interestingly, decrease of fluorescence intensity was observed in nTau titrations with all three CyDPA probes. 15 μM of CyDPA1 was used for the titration due to its low extinction coefficient in aqueous media, and showed lower binding to pTau than CyDPA2 (**Figure 5B**). The EC50 value of CyDPA1 was not calculated because the binding curve did not reach saturation at the highest pTau concentration (**Figure 5B**). The phosphate binding-induced spectroscopic changes were not found in CyDPA0 titration (data not shown).

We then studied the ratiometric signal changes upon binding between CyDPA probes and pTau protein. The ratiometric absorption was determined by absorption ratio at two different wavelengths (630/730nm for CyDPA1 and 810/750 nm for CyDPA2). Both CyDPA1 and CyDPA2 showed significantly different ratiometric results in pTau versus nTau in the buffer solution (50 mM HEPES containing 10% DMSO, pH 7.4) (**Figure 6**). The ratiometric absorption of CyDPA1 increased approximately 30% from initial to saturated pTau binding, and CyDPA2 showed a 17% increase. In nTau binding studies, however, the ratiometric absorption of CyDPA2 was decreased by 25%, and that of CyDPA1 remained unchanged throughout the tested concentrations. This data demonstrates the specific binding of CyDPA1 and CyDPA2 to pTau. CyDPA2 (EC50 = 0.27 μg/mL) showed higher binding affinity than CyDPA1 (EC50 = 1.23 μg/mL). CyDPA0, however, did not show any ratiometric absorption or fluorescnce change upon binding to pTau (data not shown). This result indicates that CyDPA1 and CyDPA2 have a great potential as ratiometric NIR probes for pTau imaging.

Next, we investigated the binding of CyDPAs to pTau in *ex vivo* samples, which were obtained and extracted from human and mouse brains. The P301L is from a mouse brain sample, and AD is from an Alzheimer's patient who had an advanced stage of Alzheimer's pathology. Both AD and P301L samples have been freshly prepared from homogenizing tissue and composed of mainly pTau proteins and aggregates with low levels of other protein species such as Aβ and alpha-synuclein oligomers [25]. Phosphorylation level of each sample was quantified by Phosphoprotein Estimation Kit, and 3.4% and 1.9% of phosphoprotein were found in AD and P301L, respectively. These samples were used for fluorescence titration studies. Enhanced fluorescence signal from CyDPA2 was observed after binding to both AD and P301L, and the titration showed a phosphate specific absorption ratio enhancement in a dose dependent manner (**Figure 7**). CyDPA1 and CyDPA0, however, did not show any significant ratiometric signal, probably due to the relatively low binding affinities. The human brain sample showed higher binding affinity (EC50 = 8.1 μg/mL) than P301L (EC50 = 12.7 μg/mL) to CyDPA2 due to higher amount of phosphorylat-

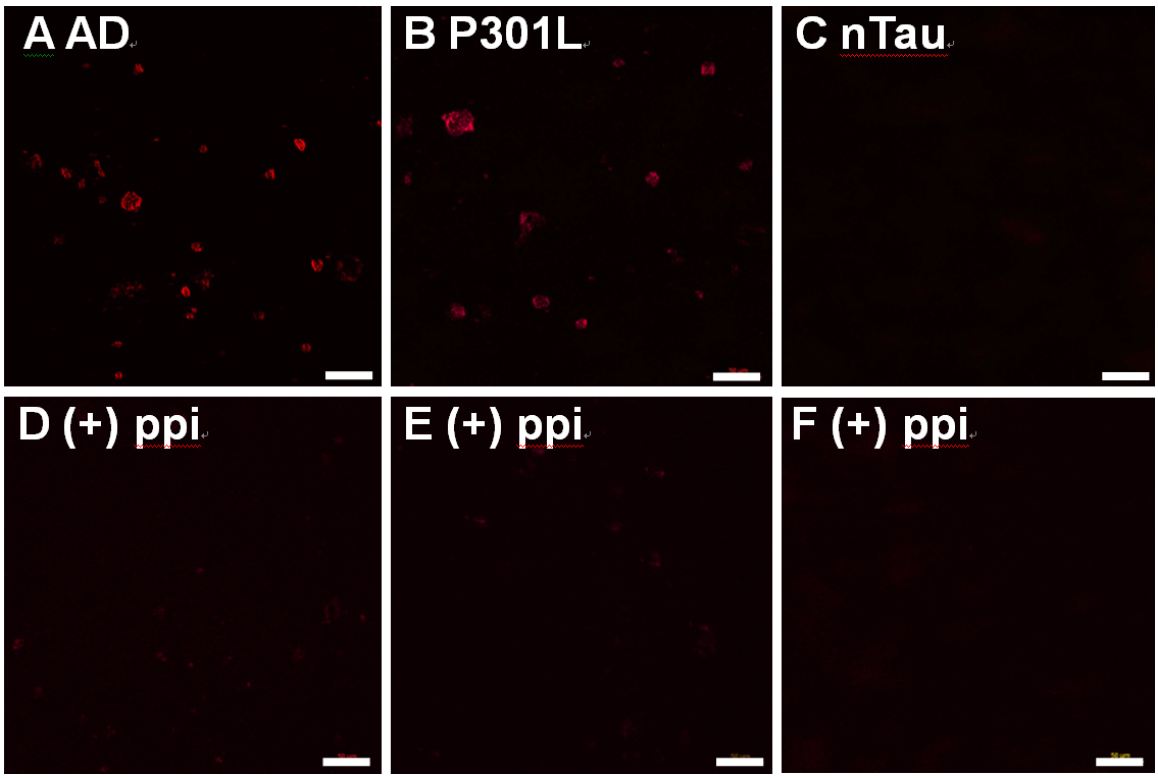

Figure 9. Fluorescence microscopy images of the brain extract samples labeled with CyDPA2 (10 μM, λ_{exi}/ λ_{emi} = 783/800 nm). In (D), (E), and (F), CyDPA2 was pretreated with 100 μM of sodium pyrophosphate (ppi). Scale bars = 50 μm. (A) AD, (B) P301L, (C) nTau protein, (D) AD + ppi, (E) P301L + ppi, and (F) nTau protein + ppi.

ed protein in AD sample. Overall, CyDPA2 appears to be the most promising probe for imaging hyperphosphorylated Tau species.

Fluorescence gel and microscopy images of Tau proteins

Gel electrophoresis was performed to visualize CyDPA-labeled pTau species. One gel was stained with ProQ diamond solution as a control phosphoprotein staining (**Figure 8A**). ProQ diamond is commonly used stain for fluorescent detection of phosphoproteins. Another gel was incubated with CyDPA2 (10 μM) in HEPES buffer for 10 min. After washing in buffer solution, the gel was imaged using Kodak In-Vivo Multispectral Imaging System with the filter set, $\lambda_{exi}/\lambda_{emi}$ = 730/790 nm (**Figure 8B**). AD, P301L, and pTau samples showed phosphorylated protein bands respectively. No significant phosphoprotein bands observed from nTau protein in neither control ProQ diamond staining nor CyDPA2-stained gels. In the lanes of AD and P301L, pTau aggregates appeared ~64 kDa which is known as a toxic hyperphosphorylated form of Tau oligomers [34, 35]. pTau species from isoforms and mutants in different sizes also showed up in AD and P301L samples. This fluorescence gel staining images suggest that CyDPA2 is specific to phosphorylated Tau.

In order to verify the specificity of CyDPA2 to Tau aggregates, microscopy studies were performed. Human AD and mouse P301L brain homogenates and nTau protein were applied and dried onto poly-L-lysine (PLL)-coated coverslips and incubated with CyDPA2 (10 μM) for 10 min. Fluorescent beads (~20 nm, λexi/λemi = 535/575 nm) were added as an internal fluorescent standard in all samples. The microscopy images (**Figure 9**) were taken using Zeiss Observer Z1 inverted microscopy equipped with an ICG filter set (λexi/λemi = 783/800 nm). In glass slides, CyDPA2-labeled protein aggregates were found at the same focal plane where the fluorescent beads were discovered. The strong fluorescent signals showed selective bindings of CyDPA2 to pTau proteins in AD and P301L, whereas no NIR fluorescence was observed from nTau protein (**Figure 9A-C**). The binding specificity of CyDPA2 to pTau species was further evidenced by a phosphate blocking

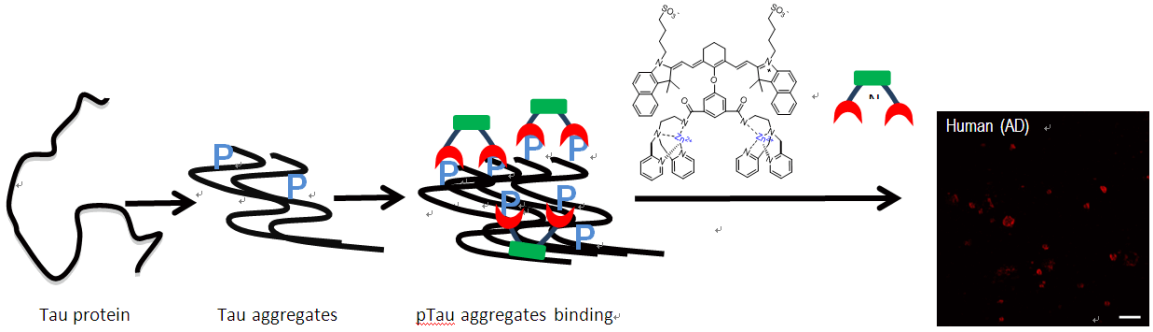

Figure 10. CyDPA Zn(II) chelates bind to hyperphosphorylated Tau aggregates. The unique in-register, parallel alignment of β-strands in Tau aggregates allows for simultaneous binding of two DPA-Zn moieties on CyDPA Zn(II) chelates.

study: the fluorescence signal was significantly reduced when *ex vivo* brain samples were treated with a mixture of CyDPA2 and pyrophosphate (ppi), a phosphate inhibitor (**Figure 9D** and **9E**).

Discussion

As a pathological hallmark of AD, NFTs have been shown to have a quantitative relationship with the degree of neurodegeneration in AD [6, 7]. However, recent studies have suggested that NFTs are not the major neurotoxic species [36, 37]. Instead, Tau aggregates, particularly Tau oligomers, which are formed at the early stage of NFTs formation and are characterized by hyperphosphorylation, could be the most toxic Tau species of all [25, 38, 39]. Abnormal phosphorylation of Tau down-regulates the protein, and is a critical component of neuronal cell death [9-11]. Therefore, Tau aggregates appear to be a potential therapeutic target for AD. Unfortunately, the exact mechanisms of Tau-mediated neurodegeneration are not well understood. Molecular imaging techniques that allow specific labeling of Tau aggregates will obviously be important in elucidating the exact roles of Tau aggregates in AD. Moreover, such imaging tools will provide opportunities in diagnosing AD at an early stage. As such, we developed the first molecular probes that allow imaging Tau aggregates using low-cost NIR fluorescence and ratiometric imaging techniques (**Figure 1**).

Our probe design has the following considerations: (1) the probe is based on a NIR fluorescent dye allowing for *in vivo* imaging applications; (2) the structures are based on ICG, the only FDA approved NIR fluorescence agent; (3) zinc dipicolylamine (DPA-Zn) moiety is incorporated into the probe to allow for binding to phosphorylated sites on Tau aggregates; (4) Upon binding, phosphate anions will introduce coordination rearrangement of the Zn ions, resulting in a ratiometric spectroscopic change; (5) In Tau aggregates, individual Tau proteins form single molecule layers, which perfectly stack on top of each other by in-register, parallel alignment of β-strands [40]. As such, phosphate groups on the same position of Tau proteins are in proximity in Tau aggregates, thus allowing for simultaneous binding of multiple DPA-Zn moieties on the same probe (**Figure 10**). DPA-Zn(II) units have been widely used as a receptor for phosphates such as ATP, phosphorylated peptides and proteins [41-44]. DPA-Zn(II) complexes have also been exploited in fluorophores and nanoparticles for phosphate labeling with high specificity and selectivity in biological systems [18, 45-49]. IR820 was used as a ICG-based parent dye and chemically coupled with DPA-Zn(II) derivatives. The rigid chlorocyclohexenyl ring in the polymethine chain of IR820 has been shown to increase photostability and enhance quantum yield in heptamethine cyanine dyes [50]. In addition, the chlorine can be easily substituted by nucleophiles such as amines, thiols, or alkoxides for functionalizations [27, 51]. In this study, we developed three DPA-Zn(II)-linked cyanine dyes to optimize pTau specific labeling of NIR dyes in AD.

The monovalent CyDPA0 and CyDPA1 were synthesized from IR820 by nucleophilic substitution reactions with DPA0 and DPA1, respectively. Compared to DPA0, ethyl amine-elongated

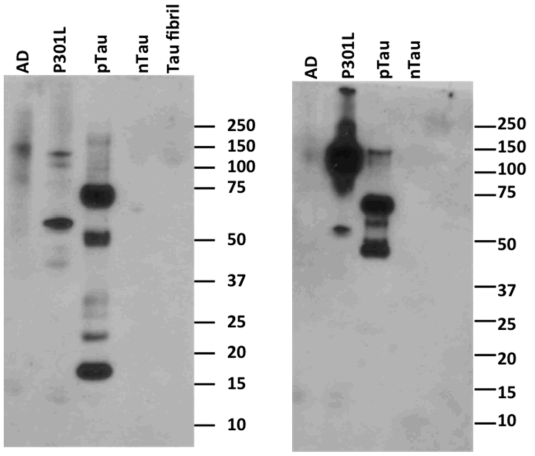

Figure 11. Western blot analysis of Tau proteins AD, P301L, pTau, nTau, and nTau firbrils probed with (A) anti-Tau S422 antibody and (B) anti-phospho Tau antibody AT8.

DPA (DPA1) has additional nitrogen for zinc coordination, therefore a stronger zinc chelator. The bivalent CyDPA2 was synthesized from two DPA-Zn(II)-conjugated phenyl hydroxide (**Figure 2**). We expected CyDPA2 to have the strongest binding to Tau aggregates as the two DPA moieties on CyDPA2 allow simultaneous binding to two phosphorylated sites.

Although all three CyDPA NIR probes were developed based on the same parent dye molecule (IR820) and have maximum absorption and emission peaks in the NIR region, they demonstrate distinctive NIR optical properties in DMSO and aqueous media (**Table 1**). CyDPA0 and CyDPA1 exhibit hypsochromicly shifted absorptions compared to the parent dye (IR820) with large Stokes shifts in both DMSO and aqueous solution. Such greatly hypsochromicly shifted absorptions and large stoke shifts have been observed in other amine-substituted tricarbocyanine derivatives [52] and are due to intramolecular charge transfer (ICT) [53]. CyDPA2, which is a hydroxyl-substituted tricarbocyanine molecule, shows similar absorption and emission as the parent dye (**Figure 3**). It is known that hydroxyl-substitution does not induce significant ICT effect on tricarbocyanine dyes [52].

We first conducted fluorescence titration studies to evaluate the binding of CyDPA probes to phosphorylated full-length Tau protein. As shown in **Figure 5B**, CyDPA1 showed dose-dependent response to pTau addition, whereas CyDPA0 did not show any significant response (data not shown). This result indicates that CyDPA1 has higher binding affinity to pTau than CyDPA0, although the EC50 value of CyDPA1 was not calculated because the binding curve did not reach saturation at the highest pTau concentration. The stronger binding of CyDAP1 to pTau may be due to, (1) the additional nitrogen for zinc-coordination in CyDPA1 can strengthen the Zn^{2+} chelation, thereby facilitating phosphate binding, and (2) the ethylamine linker in CyDPA1 may provide higher flexibility than the rigid binding pocket in CyDPA0. This allows CyDPA1 to better interact with the target phosphate groups in pTau than CyDPA0. As expected, CyDPA2 showed the highest affinity to pTau (EC50 = 0.304 μg/mL) as the two DPA-Zn(II) complexes allow simultaneous binding to two phosphorylated sites (**Figure 5**). This result indicates that the CyDPA fluorescence dye with multiple binding sites and a proper linker may enhance the binding affinity to target pTau.

In addition to fluorescence titration studies, we investigated the ratiometric signal changes upon binding of CyDPA probes to pTau protein. Absorption or fluorescence intensity measurement at one wavelength can be affected by various factors from biological microenvironment, such as pH, temperature, thickness of tissue, etc. Ratiometric measurement can provide more accurate information and exclude those influences by measuring intensities at two wavelengths. CyPDA1 showed 30% ratiometric absorption increase when treated with pTau, but no significant ratiometric change with nTau (**Figure 6B**). CyPDA2 showed 17% ratiometric absorption increase when treated with pTau, but 25% ratiometric absorption decrease with nTau. (**Figure 6A**) In addition, CyDPA2 (EC50 = 0.27 μg/mL) showed roughly four times higher binding affinity to pTau than CyDPA1 (EC50 = 1.23 μg/mL). CyDPA0, however, failed to show any significant ratiometric absorption change with pTau or nTau (data not shown). These results indicate that CyDPA1 and CyDPA2 can be potentially used to image pTau species with ratiometric imaging technique.

The binding of CyDPA probes to pTau was further evidenced in *ex vivo* brain extract samples. Up to 13% and 10% of absorption ratiometric enhancement was observed when CyDPA2 was treated with AD and P301L respectively. (**Figure**

7) Such significant ratiometric changes, however, were not observed when CyDPA1 or CyDPA0 was studied. This may be due to the fact that CyDPA2 has much higher binding affinity to pTau than the other CyDPA probes.

The relatively high ratiometric signal and binding affinity to pTau indicate that CyDPA2 is the most promising Tau probe out of the three CyDPA dyes. We therefore selected CyDPA2 for gel staining and fluorescence microscopy studies to further evaluate the potential of the probe in Tau imaging. In gel staining study, both CyDPA2 and ProQ diamond staining (positive control) labeled phosphorylated protein bands in AD, P301L and pTau samples, whereas no significant fluorescent band was observed in nTau samples (**Figure 8**). Bands at ~64 kDa in the lanes of AD and P301L correspond to a toxic hyperphosphorylated form of Tau aggregates [34, 35]. Other pTau species from isoforms and mutants in different sizes also showed up in AD and P301L. The existence of specific Tau proteins in AD and P301L were verified by western immunoblotting using antibody labeling including anti-Tau S422 antibody (specific to 45-68 kD proteins identified as Tau proteins) and anti-phospho tau antibody AT8 (labels Tau protein phosphorylated at both serine 202 and threonine 205) (**Figure 11**).

Using fluorescence microscopy, we imaged human brain (AD) and mouse brain (P301L) samples using CyDPA2 (**Figure 9**). Significant NIR fluorescence signals were observed in AD and P301L samples, and the signal was greatly reduced when phosphate blocking agent (ppi) was added. In addition, no fluorescence was observed from nTau protein. The fluorescence gel staining and fluorescence microscopy images further verified the specificity of CyDPA2 to phosphorylated Tau species.

The long-term goal of our research is clinical imaging of our Tau aggregates targeted CyDPA probes through the retina. We plan to image our Tau probes through the retina for a number of reasons: (1) It is possible to study AD through imaging Tau pathology in the retina. The retina is a direct extension of brain [54, 55], and an integral part of the central nervous system (CNS). Similar to other regions of the brain, the retina is derived from the neural tube, a precursor of the central nervous system in embryology [56]. Immunohistochemical analysis of excised human eyes indicates that hyperphosphorylated Tau aggregates are present in the retina and increases significantly with age [54]. Hyperphosphorylated Tau aggregates have also been detected in AD mouse models [57]. (2) Optical imaging of the retina is clinically translatable. Although optical imaging of the human brain is challenging due to tissue penetration, the optically transparent nature of the eye allows imaging the retina using this method. NIR fluorescence imaging of the retina has been utilized in the clinic [58-60]. (3) The common challenge of probe delivery through the blood brain barrier (BBB) can be overcome. It is usually difficult to deliver a molecular probe through the BBB to allow molecular imaging of the brain, because the probe delivery is affected by many factors such as lipid solubility, molecular weight, charge, tertiary structure and protein binding [61]. Probe delivery to the retina, however, does not face this difficulty. For these reasons, the CyDPA agents have potential in translational optical imaging of Tau aggregates through the retina.

In conclusion, we developed three NIR probes for specific labeling of Tau aggregates. Fluorescence titration studies of CyDPA2 and CyDPA1 showed pTau concentration-dependent fluorescence enhancements. In addition, both CyDPA1 and CyDPA2 demonstrated selective ratiometric absorption changes upon pTau binding. In the binding studies with *in vitro* and *ex vivo* Tau samples, we found that CyDPA2 was the most favorable NIR probe in Tau aggregates labeling with the highest binding affinity among the three probes. This specific labeling was further evidenced by images from fluorescence microscopy and gel staining. These data suggest that CyDPA2 is a promising NIR fluorescent and ratiometric imaging probe that targets Tau aggregates and has a potential in early diagnosis of AD.

Acknowledgments

The work was supported by the startup fund provided by the Department of Radiology, University of Pittsburgh, and Cullen Family Trust for Health Care and the Mitchell Center for Neurodegenerative Diseases.

Conflict of interest statement

The authors declare that they have no conflict of interest.

Address correspondence to: Dr. Mingfeng Bai, Department of Radiology, University of Pittsburgh, 100 Technology Dr., Suite 452G Pittsburgh, PA 15219. Tel: 412-624-2565; Fax: 412-624-2598; E-mail: baim@upmc.edu

References

[1] Delaère P, Duyckaerts C, Masters C, Beyreuther K, Piette F and Hauw JJ. Large amounts of neocortical βA4 deposits without neuritic plaques nor tangles in a psychometrically assessed, non-demented person. Neurosci Lett 1990; 116: 87-93.

[2] Wisniewski HM, Bancher C, Barcikowska M, Wen GY and Currie J. Spectrum of morphological appearance of amyloid deposits in Alzheimer's disease. Acta Neuropathol 1989; 78: 337-347.

[3] Rinne JO, Brooks DJ, Rossor MN, Fox NC, Bullock R, Klunk WE, Mathis CA, Blennow K, Barakos J, Okello AA, Rodriguez Martinez de Liano S, Liu E, Koller M, Gregg KM, Schenk D, Black R and Grundman M. 11C-PiB PET assessment of change in fibrillar amyloid-beta load in patients with Alzheimer's disease treated with bapineuzumab: a phase 2, double-blind, placebo-controlled, ascending-dose study. Lancet Neurol 2010; 9: 363-372.

[4] Dickson DW. Neuropathological Diagnosis of Alzheimer's Disease: A Perspective from Longitudinal Clinicopathological Studies. Neurobiol Aging 1997; 18: S21-S26.

[5] Arriagada PV, Growdon JH, Hedley-Whyte ET and Hyman BT. Neurofibrillary tangles but not senile plaques parallel duration and severity of Alzheimer's disease. Neurology 1992; 42: 631.

[6] McLean CA, Cherny RA, Fraser FW, Fuller SJ, Smith MJ, Beyreuther K, Bush AI and Masters CL. Soluble pool of Abeta amyloid as a determinant of severity of neurodegeneration in Alzheimer›s disease. Ann Neurol 1999; 46: 860-866.

[7] Duyckaerts C, Brion JP, Hauw JJ and Flament-Durand J. Quantitative assessment of the density of neurofibrillary tangles and senile plaques in senile dementia of the Alzheimer type. Comparison of immunocytochemistry with a specific antibody and Bodian›s protargol method. Acta Neuropathol 1987; 73: 167-170.

[8] Iqbal K, Alonso Adel C, Chen S, Chohan MO, El-Akkad E, Gong CX, Khatoon S, Li B, Liu F, Rahman A, Tanimukai H and Grundke-Iqbal I. Tau pathology in Alzheimer disease and other tauopathies. Biochim Biophys Acta 2005; 1739: 198-210.

[9] Ludolph AC, Sperfeld A, Collatz BM and Storch A. Tauopathies--a new class of neurodegenerative diseases. Nervenarzt 2001; 72: 78-85.

[10] Kayed R. Anti-tau oligomers passive vaccination for the treatment of Alzheimer disease. Hum Vaccin 2010; 6: 931-935.

[11] Meraz-Rios MA, Lira-De Leon KI, Campos-Pena V, De Anda-Hernandez MA and Mena-Lopez R. Tau oligomers and aggregation in Alzheimer›s disease. J Neurochem 2010; 112: 1353-1367.

[12] Ward SM, Himmelstein DS, Lancia JK and Binder LI. Tau oligomers and tau toxicity in neurodegenerative disease. Biochem Soc Trans 2012; 40: 667-671.

[13] Ballatore C, Lee VM and Trojanowski JQ. Tau-mediated neurodegeneration in Alzheimer›s disease and related disorders. Nat Rev Neurosci 2007; 8: 663-672.

[14] Haroutunian V, Davies P, Vianna C, Buxbaum JD and Purohit DP. Tau protein abnormalities associated with the progression of alzheimer disease type dementia. Neurobiol Aging 2007; 28: 1-7.

[15] Schneider A and Mandelkow E. Tau-based treatment strategies in neurodegenerative diseases. Neurotherapeutics 2008; 5: 443-457.

[16] Iqbal K, Liu F, Gong CX, Alonso Adel C and Grundke-Iqbal I. Mechanisms of tau-induced neurodegeneration. Acta Neuropathol 2009; 118: 53-69.

[17] Castillo-Carranza DL, Lasagna-Reeves CA and Kayed R. Tau aggregates as immunotherapeutic targets. Front Biosci (Schol Ed) 2013; 5: 426-438.

[18] Ojida A, Sakamoto T, Inoue M-a, Fujishima S-h, Lippens G and Hamachi I. Fluorescent BODIPY-Based Zn(II) Complex as a Molecular Probe for Selective Detection of Neurofibrillary Tangles in the Brains of Alzheimer's Disease Patients. J Am Chem Soc 2009; 131: 6543-6548.

[19] Ono M, Hayashi S, Matsumura K, Kimura H, Okamoto Y, Ihara M, Takahashi R, Mori H and Saji H. Rhodanine and Thiohydantoin Derivatives for Detecting Tau Pathology in Alzheimer's Brains. ACS Chemical Neuroscience 2011; 2: 269-275.

[20] Fodero-Tavoletti MT, Okamura N, Furumoto S, Mulligan RS, Connor AR, McLean CA, Cao D, Rigopoulos A, Cartwright GA, O'Keefe G, Gong S, Adlard PA, Barnham KJ, Rowe CC, Masters CL, Kudo Y, Cappai R, Yanai K and Villemagne VL. 18F-THK523: a novel in vivo tau imaging ligand for Alzheimer's disease. Brain 2011; 134: 1089-1100.

[21] Frangioni JV. In vivo near-infrared fluorescence imaging. Curr Opin Chem Biol 2003; 7: 626-634.

[22] Ojida A, Nonaka H, Miyahara Y, Tamaru SI, Sada K and Hamachi I. Bis(Dpa-Zn-II) append-

ed xanthone: Excitation ratiometric chemosensor for phosphate anions. Angew Chem Int Edit 2006; 45: 5518-5521.

[23] Lasagna-Reeves CA, Castillo-Carranza DL, Sengupta U, Clos AL, Jackson GR and Kayed R. Tau oligomers impair memory and induce synaptic and mitochondrial dysfunction in wild-type mice. Mol Neurodegener 2011; 6: 39.

[24] Lewis J, McGowan E, Rockwood J, Melrose H, Nacharaju P, Van Slegtenhorst M, Gwinn-Hardy K, Paul Murphy M, Baker M, Yu X, Duff K, Hardy J, Corral A, Lin WL, Yen SH, Dickson DW, Davies P and Hutton M. Neurofibrillary tangles, amyotrophy and progressive motor disturbance in mice expressing mutant (P301L) tau protein. Nat Genet 2000; 25: 402-405.

[25] Lasagna-Reeves CA, Castillo-Carranza DL, Sengupta U, Sarmiento J, Troncoso J, Jackson GR and Kayed R. Identification of oligomers at early stages of tau aggregation in Alzheimer's disease. Faseb J 2012; 26: 1946-1959.

[26] Xia J, Wang Y, Li G, Yu J and Yin D. Synthesis of pyridyl derivatives for the future functionalization of biomolecules labeled with the fac-[^{188}Re$(CO)_3(H_2O)_3$]+; precursor. Journal of Radioanalytical and Nuclear Chemistry 2009; 279: 245-252.

[27] Flanagan JH, Khan SH, Menchen S, Soper SA and Hammer RP. Functionalized Tricarbocyanine Dyes as Near-Infrared Fluorescent Probes for Biomolecules. Bioconjug Chem 1997; 8: 751-756.

[28] Megens RP, van den Berg TA, de Bruijn AD, Feringa BL and Roelfes G. Multinuclear Non-Heme Iron Complexes for Double-Strand DNA Cleavage. Chemistry 2009; 15: 1723-1733.

[29] Tang B, Huang H, Xu K, Tong L, Yang G, Liu X and An L. Highly sensitive and selective near-infrared fluorescent probe for zinc and its application to macrophage cells. Chem Commun (Camb) 2006; 3609-3611.

[30] Kiyose K, Kojima H, Urano Y and Nagano T. Development of a Ratiometric Fluorescent Zinc Ion Probe in Near-Infrared Region, Based on Tricarbocyanine Chromophore. J Am Chem Soc 2006; 128: 6548-6549.

[31] Ishida Y, Inoue M-a, Inoue T, Ojida A and Hamachi I. Sequence selective dual-emission detection of (i, i + 1) bis-phosphorylated peptide using diazastilbene-type Zn(ii)-Dpa chemosensor. Chem Commun (Camb) 2009; 2848-2850.

[32] Maruyama S, Kikuchi K, Hirano T, Urano Y and Nagano T. A Novel, Cell-Permeable, Fluorescent Probe for Ratiometric Imaging of Zinc Ion. J Am Chem Soc 2002; 124: 10650-10651.

[33] Strekowski L, Lipowska M and Patonay G. Substitution reactions of a nucleofugal group in heptamethine cyanine dyes. Synthesis of an isothiocyanato derivative for labeling of proteins with a near-infrared chromophore. J Org Chem 1992; 57: 4578-4580.

[34] Ramsden M, Kotilinek L, Forster C, Paulson J, McGowan E, SantaCruz K, Guimaraes A, Yue M, Lewis J, Carlson G, Hutton M and Ashe KH. Age-dependent neurofibrillary tangle formation, neuron loss, and memory impairment in a mouse model of human tauopathy (P301L). J Neurosci 2005; 25: 10637-10647.

[35] Guerrero R, Navarro P, Gallego E, Garcia-Cabrero AM, Avila J and Sanchez MP. Hyperphosphorylated tau aggregates in the cortex and hippocampus of transgenic mice with mutant human FTDP-17 Tau and lacking the PARK2 gene. Acta Neuropathol 2009; 117: 159-168.

[36] Berger Z, Roder H, Hanna A, Carlson A, Rangachari V, Yue M, Wszolek Z, Ashe K, Knight J, Dickson D, Andorfer C, Rosenberry TL, Lewis J, Hutton M and Janus C. Accumulation of pathological tau species and memory loss in a conditional model of tauopathy. J Neurosci 2007; 27: 3650-3662.

[37] Patterson KR, Remmers C, Fu Y, Brooker S, Kanaan NM, Vana L, Ward S, Reyes JF, Philibert K, Glucksman MJ and Binder LI. Characterization of prefibrillar Tau oligomers in vitro and in Alzheimer disease. J Biol Chem 2011; 286: 23063-23076.

[38] Henkins KM, Sokolow S, Miller CA, Vinters HV, Poon W, Cornwell LB, Saing T and Gylys KH. Extensive p-Tau Pathology and SDS-Stable p-Tau Oligomers in Alzheimer's Cortical Synapses. Brain Pathol 2012; 22: 826-33.

[39] Patterson KR, Remmers C, Fu Y, Brooker S, Kanaan NM, Vana L, Ward S, Reyes JF, Philibert K, Glucksman MJ and Binder LI. Characterization of prefibrillar Tau oligomers in vitro and in Alzheimer disease. J Biol Chem 2011; 286: 23063-23076.

[40] Margittai M and Langen R. Template-assisted filament growth by parallel stacking of tau. Proc Natl Acad Sci U S A 2004; 101: 10278-10283.

[41] Sakamoto T, Ojida A and Hamachi I. Molecular recognition, fluorescence sensing, and biological assay of phosphate anion derivatives using artificial Zn(ii)-Dpa complexes. Chem Commun (Camb) 2009; 141-152.

[42] Tamaru Si and Hamachi I. Recent Progress of Phosphate Derivatives Recognition Utilizing Artificial Small Molecular Receptors in Aqueous Media Recognition of Anions. In: Vilar R, editors. Springer Berlin: Heidelberg; 2008. pp: 95-125.

[43] Ojida A, Honda K, Shinmi D, Kiyonaka S, Mori Y and Hamachi I. Oligo-Asp Tag/Zn(II) Complex Probe as a New Pair for Labeling and Fluorescence Imaging of Proteins. J Am Chem Soc 2006; 128: 10452-10459.

[44] Park C and Hong JI. A new fluorescent sensor for the detection of pyrophosphate based on a tetraphenylethylene moiety. Tetrahedron Lett 2010; 51: 1960-1962.
[45] Moro AJ, Schmidt J, Doussineau T, Lapresta-Fernandez A, Wegener J and Mohr GJ. Surface-functionalized fluorescent silica nanoparticles for the detection of ATP. Chem Commun (Camb) 2011; 47: 6066-6068.
[46] Chakkumkumarath L, Hanshaw RG and Smith BD. Zn(II)-dipicolylamine coordination complexes as sensors for phosphatidylserine containing membranes. Abstr Pap Am Chem S 2004; 228: U69-U69.
[47] Lakshmi C, Hanshaw RG and Smith BD. Fluorophore-linked zinc(II)dipicolylamine coordination complexes as sensors for phosphatidylserine-containing membranes. Tetrahedron 2004; 60: 11307-11315.
[48] Ojida A, Takashima I, Kohira T, Nonaka H and Hamachi I. Turn-On Fluorescence Sensing of Nucleoside Polyphosphates Using a Xanthene-Based Zn(II) Complex Chemosensor. J Am Chem Soc 2008; 130: 12095-12101.
[49] Leevy WM, Gammon ST, Johnson JR, Lampkins AJ, Jiang H, Marquez M, Piwnica-Worms D, Suckow MA and Smith BD. Noninvasive Optical Imaging of Staphylococcus aureus Bacterial Infection in Living Mice Using a Bis-Dipicolylamine-Zinc(II) Affinity Group Conjugated to a Near-Infrared Fluorophore. Bioconjug Chem 2008; 19: 686-692.
[50] Zhang Z and Achilefu S. Synthesis and evaluation of polyhydroxylated near-infrared carbocyanine molecular probes. Org Lett 2004; 6: 2067-2070.
[51] Boyer AE, Devanathan S, Hamilton D and Patonay G. Spectroscopic studies of a near-infrared absorbing pH sensitive carbocyanine dye. Talanta 1992; 39: 505-510.
[52] Kiyose K, Aizawa S, Sasaki E, Kojima H, Hanaoka K, Terai T, Urano Y and Nagano T. Molecular design strategies for near-infrared ratiometric fluorescent probes based on the unique spectral properties of aminocyanines. Chemistry 2009; 15: 9191-9200.
[53] Peng X, Song F, Lu E, Wang Y, Zhou W, Fan J and Gao Y. Heptamethine Cyanine Dyes with a Large Stokes Shift and Strong Fluorescence: A Paradigm for Excited-State Intramolecular Charge Transfer. J Am Chem Soc 2005; 127: 4170-4171.
[54] Leger F, Fernagut PO, Canron MH, Leoni S, Vital C, Tison F, Bezard E and Vital A. Protein aggregation in the aging retina. J Neuropathol Exp Neurol 2011; 70: 63-68.
[55] Koronyo-Hamaoui M, Koronyo Y, Ljubimov AV, Miller CA, Ko MK, Black KL, Schwartz M and Farkas DL. Identification of amyloid plaques in retinas from Alzheimer's patients and noninvasive in vivo optical imaging of retinal plaques in a mouse model. Neuroimage 2011; 54: S204-S217.
[56] Guo L, Duggan J and Cordeiro MF. Alzheimer's disease and retinal neurodegeneration. Curr Alzheimer Res 2010; 7: 3-14.
[57] Chiu K, Chan TF, Wu A, Leung IY, So KF and Chang RC. Neurodegeneration of the retina in mouse models of Alzheimer's disease: what can we learn from the retina? Age (Dordr) 2012; 34: 633-649.
[58] Gomi F and Tano Y. Polypoidal choroidal vasculopathy and treatments. Curr Opin Ophthalmol 2008; 19: 208-212.
[59] Rosen RB, Hathaway M, Rogers J, Pedro J, Garcia P, Dobre GM and Podoleanu AG. Simultaneous OCT/SLO/ICG imaging. Invest Ophthalmol Vis Sci 2009; 50: 851-860.
[60] Schmidt-Erfurth U, Teschner S, Noack J and Birngruber R. Three-dimensional topographic angiography in chorioretinal vascular disease. Invest Ophthalmol Vis Sci 2001; 42: 2386-2394.
[61] Banks WA. Characteristics of compounds that cross the blood-brain barrier. BMC Neurol 2009; 9 Suppl 1: S3.